Chinese Journal of Natural Medicines

Activation of LONP1 by 84–B10 alleviates aristolochic acid nephropathy *via* re–establishing mitochondrial and peroxisomal homeostasis

Xinyue XU, Wenping ZHU, Mengqiu MIAO, Mi BAI, Jiaojiao FAN, Yujia NIU, Yuting LI, Aihua ZHANG, Zhanjun JIA, Mengqiu WU

Citation: Xinyue XU, Wenping ZHU, Mengqiu MIAO, Mi BAI, Jiaojiao FAN, Yujia NIU, Yuting LI, Aihua ZHANG, Zhanjun JIA, Mengqiu WU, Activation of LONP1 by 84–B10 alleviates aristolochic acid nephropathy *via* re–establishing mitochondrial and peroxisomal homeostasis, Chinese Journal of Natural Medicines, 2024, 22(9), 808–821. doi: 10.1016/S1875–5364(24)60608–4.

View online: https://doi.org/10.1016/S1875–5364(24)60608–4

Available online at www.sciencedirect.com
ScienceDirect
Chinese Journal of Natural Medicines 2024, **22**(9): 808-821
doi: 10.1016/S1875-5364(24)60608-4
Chinese Journal of Natural Medicines

•Original article•

Activation of LONP1 by 84-B10 alleviates aristolochic acid nephropathy *via* re-establishing mitochondrial and peroxisomal homeostasis

XU Xinyue[1, 2, 3, 4], ZHU Wenping[2, 3, 4], MIAO Mengqiu[2, 3, 4], BAI Mi[2, 3, 4], FAN Jiaojiao[1, 2, 3, 4], NIU Yujia[3, 4], LI Yuting[2, 3, 4], ZHANG Aihua[1, 2, 3, 4*], JIA Zhanjun[2, 3, 4*], WU Mengqiu[2, 3, 4*]

[1] *School of Medicine, Southeast University, Nanjing 210009, China;*
[2] *Department of Nephrology, Children's Hospital of Nanjing Medical University, Nanjing 210008, China;*
[3] *Nanjing Key Laboratory of Pediatrics, Children's Hospital of Nanjing Medical University, Nanjing 210008, China;*
[4] *Jiangsu Key Laboratory of Early Development and Chronic Diseases Prevention in Children, Nanjing Medical University, Nanjing 210029, China*

Available online 20 Sep., 2024

[ABSTRACT] Pharmaceutical formulations derived from Aristolochiaceae herbs, which contain aristolochic acids (AAs), are widely used for medicinal purposes. However, exposure to these plants and isolated AAs is linked to renal toxicity, known as AA nephropathy (AAN). Currently, the mechanisms underlying AAN are not fully understood, leading to unsatisfactory treatment strategies. In this study, we explored the protective role of 84-B10 (5-[[2-(4-methoxyphenoxy)-5-(trifluoromethyl) phenyl] amino]-5-oxo-3-phenylpentanoic acid) against AAN. RNA-seq analysis revealed that the mitochondrion and peroxisome were the most affected cellular components following 84-B10 treatment in AAN mice. Consistently, 84-B10 treatment preserved mitochondrial ultrastructure, restored mitochondrial respiration, enhanced the expression of key transporters (carnitine palmitoyltransferase 2) and enzymes (acyl-Coenzyme A dehydrogenase, medium chain) involved in mitochondrial fatty acid β-oxidation, and reduced mitochondrial ROS generation in both aristolochic acid I (AAI)-challenged mice kidneys and cultured proximal tubular epithelial cells. Additionally, 84-B10 treatment increased the expression of key transporters (ATP binding cassette subfamily D) and rate-limiting enzymes (acyl-CoA oxidase 1) involved in peroxisomal fatty acid β-oxidation and restored peroxisomal redox balance. Knocking down LONP1 expression diminished the protective effects of 84-B10 against AAN, suggesting LONP1-dependent protection. In conclusion, our study provides evidence that AAN is associated with significant disturbances in both mitochondrial and peroxisomal functions. The LONP1 activator 84-B10 demonstrates therapeutic potential against AAN, likely by maintaining homeostasis in both mitochondria and peroxisomes.

[KEY WORDS] Aristolochic acid nephropathy; 84-B10; LONP1; Mitochondrion; Peroxisome
[CLC Number] R965 **[Document code]** A **[Article ID]** 2095-6975(2024)09-0808-14

Introduction

Aristolochic acids (AAs) are a group of structurally related nitrophenanthrene carboxylic acids derived from plants of the Aristolochiaceae family, with aristolochic acid I (AAI) and aristolochic acid II (AAII) being their primary constituents [1, 2]. These herbs have demonstrated various pharmacological activities, including anti-inflammatory, anti-malarial, and anti-hyperglycemic effects [3, 4]. For decades, pharmaceutical formulations containing Aristolochiaceae herbs have been utilized globally to treat a range of ailments, such as hepatitis, upper respiratory tract infections, pneumonia, urinary tract infections, arthralgia, hypertension, heart failure, and festering wounds [3]. However, the use of these AA-containing formulations poses significant health risks due to their

[Received on] 09-Feb.-2024
[Research funding] This work was supported by the National Key Research and Development Program of China (Nos. 2019YFA0802-702-1, 2022YFC2705100, 2022YFC2705105), the National Natural Science Foundation of China (Nos. 82070701, 82090022, and 8183-0020), the Natural Science Foundation of Jiangsu Province (No. BK 20231130), the Social Development Foundation of Jiangsu Province (No. BE2021607), the "333" Talent Plan of Jiangsu Province (No. 333-2022001), the Medical Research Project from Jiangsu Health and Health Commission (No. Z2022071), and the Outstanding Youth Project from Nanjing Health and Health Commission (No. JQX22010).
[*]**Corresponding author]** E-mails: zhaihua@njmu.edu.cn (ZHANG Aihua); jiazj72@hotmail.com (JIA Zhanjun); mengqiuwu@njmu.edu.cn (WU Mengqiu)
These authors have no conflict of interest to declare.

nephrotoxicity, resulting in a condition known as aristolochic acid nephropathy (AAN) [5, 6]. AAN is characterized by elevated serum creatinine (sCr) levels, rapid tubulointerstitial injury, and loss of renal proximal tubules, often leading to chronic kidney disease and end-stage renal disease [7]. Despite extensive research, the underlying mechanisms of AAN remain poorly understood, hindering the development of effective treatment strategies.

AAs exert their primary toxic effects on tubular epithelial cells, which selectively reabsorb these compounds through specific organic anion transporters [8-10]. Previous studies have shown that AAs induce mitochondrial damage and oxidative stress within these cells [11, 12]. This mitochondrial dysfunction may result from the direct binding of AAs to key proteins essential for maintaining mitochondrial homeostasis [2]. Consequently, mitochondria have been identified as potential therapeutic targets. Additionally, peroxisomes, single membrane-bound organelles lacking DNA, play crucial roles in cellular metabolism, including fatty acid *β*-oxidation (FAO) and redox homeostasis, functions they share with mitochondria [13, 14]. Peroxisomes are also involved in ether phospholipid biosynthesis, bile acid synthesis, docosahexaenoic acid synthesis, glyoxylate metabolism, and amino acid degradation [15-18]. Given the kidney's high metabolic activity and its reliance on both mitochondria and peroxisomes for normal function, it is not surprising that peroxisomal dysfunction is observed in acute kidney injuries caused by sepsis and ischemia [19, 20]. Therefore, developing strategies to preserve peroxisomal function is also crucial for effective kidney injury therapy.

Studies have indicated that peroxisomes rely on ongoing interactions with other organelles, particularly mitochondria, to fulfill their intrinsic metabolic roles [21]. However, the specific signaling pathways facilitating communication between peroxisomes and mitochondria remain poorly understood. Recent research has highlighted that one mechanism of interorganelle communication involves physical contact [22, 23]. It is well established that mitochondria are interconnected with the endoplasmic reticulum (ER) *via* mitochondria-associated ER membranes (MAMs). Additionally, studies have shown that peroxisomes preferentially localize to mitochondria at MAM sites through direct interaction between the peroxisomal membrane protein Pex11 and the ER-mitochondria encounter structure (ERMES) component Mdm34 [23, 24]. Intriguingly, recent research in mouse cardiomyocytes identified mitochondrial Lon protease (LONP1), a highly conserved ATP-dependent protease crucial for maintaining mitochondrial proteostasis, as a new component of MAMs [25]. This finding suggests a potential role for LONP1 in mediating mitochondria-peroxisome interactions. Based on this evidence, it is reasonable to hypothesize that stabilizing or activating LONP1 may protect against AAN by preserving the homeostasis of both mitochondria and peroxisomes.

In our previous investigations, we identified a novel 3-phenylglutaric acid derivative, 84-B10 (5-[[2-(4-methoxyphenoxy)-5-(trifluoromethyl) phenyl] amino]-5-oxo-3-phenylpentanoic acid), characterized by CAS number: 698346-43-9, as a potent LONP1 activator [26]. This compound was shown to provide protection against renal tubular fibrosis and cisplatin-induced acute kidney injury by restoring mitochondrial homeostasis [26-28]. Remarkably, in our current study, we found that 84-B10 not only effectively improved mitochondrial homeostasis but also partially restored peroxisome homeostasis in an AAN model, concomitant with enhanced LONP1 expression. Notably, the protective effects of 84-B10 were significantly diminished following LONP1 knockdown. These findings strongly suggest that activation of LONP1 may protect against AAN by promoting structural and functional stability of mitochondria and indirectly supporting peroxisomal homeostasis through enhanced mitochondria-peroxisome interactions. In conclusion, our study provides valuable insights into the pathophysiology of AAN and underscores the therapeutic potential of the novel 3-phenylglutaric acid derivative, 84-B10, in the prevention and treatment of AAN.

Materials and Method

Chemicals and reagents

The compound 84-B10 was synthesized by Shanghai Medicilon Inc. (purity ≥ 99%, Shanghai, China). Aristolochic acid I (AAI) was purchased from Sigma-Aldrich (purity ≥ 90%, Cat#A5512, St Louis, MO, USA). Both compounds were dissolved in dimethyl sulfoxide (DMSO) (purity ≥ 99%, Cat#V900090, Sigma-Aldrich).

Animal experiments

C57BL/6J male mice (8 weeks old) were obtained from GemPharmatech Co., Ltd. (Nanjing, China). They were housed in a specific pathogen-free environment with a 12-hour light-dark cycle and a temperature maintained between 20−24 °C. The mice had free access to food and water.

To investigate the impact of 84-B10 on AAN, the mice were randomly divided into three groups: the vehicle group, AAI group, and AAI + 84-B10 group. AAN group of mice were induced by intraperitoneal (i.p.) injection of AAI at a dosage of 5 mg·kg^{-1} for five consecutive days. In the AAI + 84-B10 group, mice were pre-treated with 84-B10 (10 mg·kg^{-1}) 24 and 48 h before the first AAI injection and then received daily 84-B10 administration (10 mg·kg^{-1}) before the AAI injection. Mice in the vehicle and AAI groups were given an equivalent volume of 10% DMSO in saline once daily. All mice were euthanized five days after the AAI injection, and both whole blood and kidney tissues were collected (Fig. 1A). The animal experiments were conducted with approval from the Institutional Animal Care and Use Committee at Nanjing Medical University, registered under the number IACUC 2007001.

Serum biochemical analysis

Whole blood samples were centrifuged at 4000 r·min^{-1} for 20 min, and the resulting supernatant was collected for biochemical analysis. The levels of blood urea nitrogen (BUN) and sCr were determined using a Hitachi 7600 analyz-

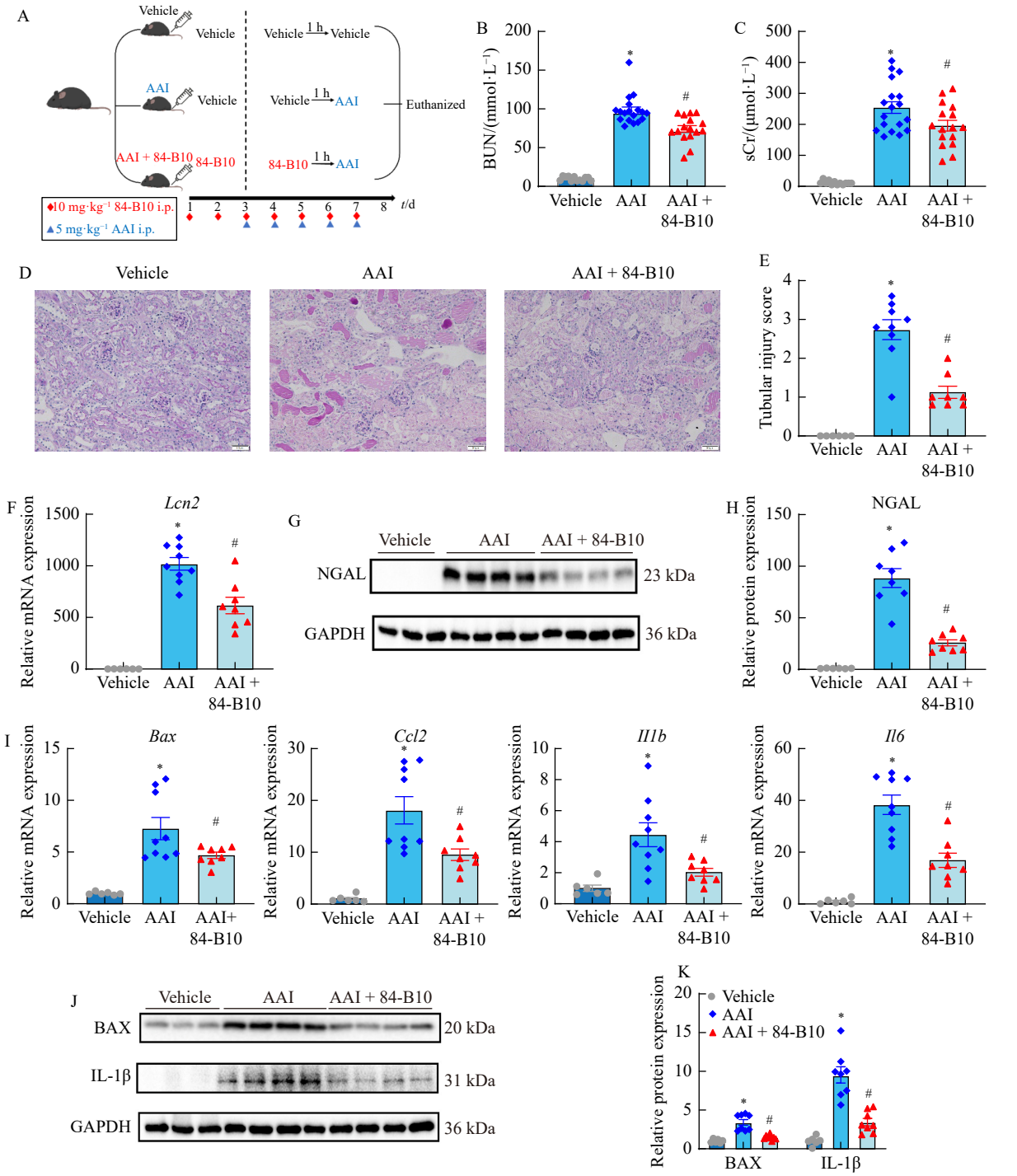

Fig. 1 84-B10 significantly alleviated kidney injury, apoptosis, and inflammation in AAN mice. (A) Schematic representation of the experimental groups and administration regimen. (B–C) Measurement of BUN and sCr levels in mouse serum (n = 12–18). (D) Representative images of kidney tissue sections stained with PAS. Scale bar = 50 μm. (E) Quantification of tubular injury scores based on PAS staining. (F) mRNA expression levels of *Lcn2* (encoding NGAL) in kidney tissues (n = 6–9). (G–H) Representative Western blots and semi-quantification of NGAL protein levels in kidney tissues (n = 6–8). (I) mRNA expression levels of *Bax*, *Ccl2*, *Il1b*, and *Il6* in kidney tissues (n = 6–9). (J–K) Western blotting analysis of BAX and IL-1β protein levels in kidney tissues, with semi-quantification shown in (K) (n = 6–8). Data are presented as mean ± SEM. $^{*}P < 0.05$ *vs* the vehicle group; $^{\#}P < 0.05$ *vs* the AAI group.

er (Hitachi, Tokyo, Japan).

Periodic acid-Schiff (PAS) staining

The PAS staining procedure was conducted using a commercially available kit (Cat#G1281, Solarbio, Wuhan, China) following the manufacturer's instructions. After staining, the sections were observed and captured using an Olympus BX51

microscope (Olympus, Center Valley, PA, USA). The tubular injury score was evaluated by a blinded pathologist according to the following criteria: score 0, no abnormalities; score 1, less than 25% abnormalities; score 2, 25% to 50% abnormalities; score 3, 50% to 75% abnormalities; score 4, more than 75% abnormalities.

RNA-seq analysis

Fresh kidney tissues were collected from the three groups for RNA-seq analysis. The procedure involved the extraction of total RNA, isolation of mRNA, and PCR amplification. The resulting library products were sequenced using a BGISEQ-500 sequencer. Differentially expressed genes were defined as having a fold change ≥ 1.5 or ≤ 0.67 with a *Q*-value < 0.05. Gene Ontology (GO) enrichment analysis, Kyoto Encyclopedia of Genes and Genomes (KEGG) enrichment analysis, and gene set enrichment analysis (GSEA) were performed using the online tool provided by the Beijing Genomics Institute, accessible at https://biosys.bgi.com. The raw data file and processed data of transcriptional analysis have been submitted to the NCBI Gene Expression Omnibus (GEO) database and can be accessed under the identifier GSE245755. Access to these data is granted through a secure token number: wjuveiuidtifhul.

Cell culture and treatment

Mouse kidney proximal tubular epithelial cells (TKPT) were procured from the American Type Culture Collection (ATCC, Manassas, VA, USA) and cultured at 37 °C in Dulbecco's Modified Eagle Medium (DMEM)/F12 medium (Cat#C11330500BT, Gibco, CA, USA). The medium was supplemented with 7% (*V/V*) fetal bovine serum (FBS) (Cat#ST30-3302, PAN Biotech, Germany), 0.003% (*W/V*) insulin (Cat#P3376-400IU, Beyotime, Shanghai, China), 100 $U \cdot mL^{-1}$ penicillin, 100 $\mu g \cdot mL^{-1}$ streptomycin, and 5% CO_2.

Western blotting analysis

Kidney tissues and TKPT cells were fully lysed using RIPA lysate (Cat#P0045, Beyotime) with the addition of protease inhibitors (Cat#4693116001, Roche, USA). Total protein levels were quantified using the bicinchoninic acid (BCA) assay. Equal protein amounts from each sample were loaded and separated by sodium dodecyl sulfate-polyacrylamide gel electrophoresis (SDS-PAGE). Subsequently, proteins were transferred onto methanol-activated polyvinylidene fluoride (PVDF) membranes. The PVDF membranes were blocked with 5% non-fat milk powder for 1 h at room temperature and then incubated with primary antibodies overnight at 4 °C. The primary antibodies used included: neutrophil gelatinase-associated lipocalin (NGAL) polyclonal antibody (1 ∶ 1000, Cat#ab63929, Abcam, Cambridge, MA, USA); BCL2-associated X protein (BAX) polyclonal antibody (1 ∶ 1000, Cat#50599-2-Ig, Proteintech); interleukin 1β (IL-1β) antibody (1 ∶ 1000, Cat#A16288, ABclonal, Wuhan, China); acyl-Coenzyme A dehydrogenase, medium chain (ACADM) polyclonal antibody (1 ∶ 1000, Cat#55210-1-AP, Proteintech, Rosemont, IL, USA); superoxide dismutase 2 (SOD2) (1 ∶ 1000, Cat#13533, Abcam); carnitine palmitoyltransferase 2 (CPT2) monoclonal antibody (1 ∶ 500, Cat#ET1611-64, Huabio, Hangzhou, China); acyl-CoA oxidase 1 (ACOX1) monoclonal antibody (1 ∶ 1000, Cat#68017-1-Ig, Proteintech); Catalase monoclonal antibody (1 ∶ 2000, Cat#66765-1-Ig, Proteintech); ATP binding cassette subfamily D member 3 (ABCD3) monoclonal antibody (1 ∶ 1000, Cat#66697-1-Ig, Proteintech); monoclonal complex II subunit SDHB antibody (C II-SDHB) (1 ∶ 1000, Cat#ab14714, Abcam); monoclonal complex III subunit UQCRC2 (C III-UQCRC2) antibody (1 ∶ 1000, Cat#ab14745, Abcam); monoclonal complex V subunit ATP5A antibody (C V-ATP5A) (1 ∶ 1000, Cat# ab14748, Abcam); LONP1 antibody (1 ∶ 1000, Cat#A4293, ABclonal); monoclonal 3-hydroxy-3-methylglutaryl-CoA synthase 2 (HMGCS2) antibody (1 ∶ 1000, Cat# 20940, Cell Signaling Technology); glyceraldehyde-3-phosphate dehydrogenase (GAPDH) monoclonal antibody (1 ∶ 2000, Cat#60004-1-Ig, Proteintech); β-actin monoclonal antibody (1 ∶ 2000, Cat#66009-1-Ig, Proteintech). Afterward, the PVDF membranes were incubated with peroxidase-tagged secondary antibodies for 1 hour at room temperature. The resulting immunoreactive bands were detected using a chemiluminescence kit (Cat#PA112, Tiangen Biotech, Beijing, China) with the Bio-Rad ChemiDoc XRS+ System (Hercules, CA, USA). Quantification of the bands was carried out using Image J software (National Institutes of Health, Bethesda, Maryland, USA).

Quantitative real-time polymerase chain reaction (qRT-PCR)

Total RNA from both kidney tissues and TKPT cells was extracted using RNAiso Plus (Cat#9109, Takara Biotechnology, Dalian, China). The extracted RNA was reverse transcribed into cDNA using Reverse Transcriptase M-MLV (Cat#2641A, Takara Biotechnology) following the manufacturer's protocol. Quantitative PCR was subsequently performed using SYBR Green Master Mix (Cat#Q131-02, Vazyme, Nanjing, China) on a Step One Plus PCR System (Applied Biosystems). The specific primers used for the qRT-PCR are listed in Table S1.

Cell viability assay

The cell counting kit-8 (CCK-8) (Cat#K1018, ApexBio, Houston, TX, USA) was used to assess cell viability. Briefly, TKPT cells were seeded in a 96-well plate and stimulated with the indicated concentrations of AAI and/or 84-B10. After the treatment, 10 microliters of the CCK-8 reagent were added to each well and incubated for 1 hour at 37 °C. The absorbance was measured at 450 nm. Relative cell viability was compared with that of the control group to evaluate the impact of the treatments on cell viability.

Total cellular ROS and mitochondrial ROS (mtROS) analysis

Live TKPT cells were incubated with 2',7'-dichlorofluorescin diacetate (Cat#S0033S, Beyotime) at 37 °C for 20 minutes to estimate total cellular ROS or incubated with MitoSOX™ Red (Cat#M36008, Invitrogen, CA, USA) at 37 °C for 30 minutes to estimate mtROS levels. After incubation, cells were digested with trypsin and subjected to fluorescence intensity analysis on a CytoFLEX flow cytometer (Beckman Coulter Life Sciences, Nyon, Switzerland).

Mitochondrial DNA (mtDNA) copy number analysis

Total DNA from TKPT cells was extracted using the TIANamp Genomic DNA Kit (Cat#DP304, Tiangen Biotech) following the manufacturer's instructions. Quantitative PCR was utilized to detect the copy number of a specific mitochondrial gene, *mt-Co2*. Relative mtDNA copy numbers were normalized to that of the nuclear 18S rRNA gene. The primers used for the analysis of mouse *mt-Co2* were F: 5'-GCCGACTAAATCAAGCAACA-3' and R: 5'-CAATGGGCATAAAGCTATGG-3'. The primers for mouse *18S rRNA* were F: 5'-TTCGGAACTGAGGCCATGATT-3' and R: 5'-TTTCGCTCTGGTCCGTCTTG-3'.

Mitochondrial ultrastructure analysis

Kidney samples were harvested and immersed in a solution of 2.5% glutaraldehyde in 0.1 mol·L^{-1} sodium cacodylate buffer for more than 2 hours. After glutaraldehyde fixation, the samples were further fixed with 1% osmium tetroxide (OsO4). Ultrathin sections (60−80 nm thickness) were prepared and stained with 2% acetic acid dioxygen and 3% lead citrate. The staining enhances the contrast of cellular structures in the transmission electron microscope (TEM). Finally, the stained ultrathin sections were observed using a JEM 1400 TEM (Japan Electron Optics Laboratory Co., Ltd., Tokyo, Japan). To quantify mitochondrial injury, a scoring system was employed with the following criteria: score 0, no injury observed; score 1, slight decrease of cristae or the presence of small vacuoles; score 2, severe decrease of cristae or the presence of big vacuoles; score 3, severe decrease of cristae, presence of large vacuoles formation and myelin figures.

Immunofluorescence staining

Mouse kidney sections were conventionally dewaxed and rehydrated, followed by microwave heating in citrate antigen repair solution (Cat#P0083, Beyotime) for 20 minutes. Subsequently, the sections were blocked with a solution consisting of 5% goat serum and 0.3% Triton X-100 in PBS for 1 hour at room temperature. The sections were then incubated with the primary antibody against LONP1 (1 ∶ 100, Cat#A4293, ABclonal) overnight at 4 °C. The following day, an Alexa Fluor 488-conjugated goat anti-rabbit IgG secondary antibody (1 ∶ 1000, Cat#ab150077, Abcam) was applied. Cell nuclei were labeled with 4',6-diamidino-2-phenylindole (DAPI). After washing with PBS/T three times, the sections were viewed and imaged using an Olympus BX51 microscope (Olympus, Tokyo, Japan).

Hydrogen peroxide (H_2O_2) concentration analysis

A commercial H_2O_2 assay kit (Cat#BC3595, Solarbio, Beijing, China) was used to assess H_2O_2 levels in TKPT cell samples. The absorbance of each sample was measured at a wavelength of 415 nm.

RNA interference

TKPT cells were transfected with scrambled small interfering RNA (siRNAs) or siRNAs targeting mouse *Lonp1* (Cat#siG1512031128-28/34/41, RiboBio, Guangzhou, China) using Lipofectamine 2000 transfection reagent (Cat#1166-8500, ThermoFisher, IL, USA) according to the manufacturer's instructions

Statistical analysis

All data were expressed as mean ± standard error of the mean (SEM). An unpaired Student's *t*-test was used for comparisons involving a single variable, and analysis of variance (ANOVA) was employed for comparisons involving two variables. A *P*-value of < 0.05 was considered statistically significant.

Results

84-B10 significantly alleviated AAN in mice

Firstly, the therapeutic effect of 84-B10 was confirmed in AAI-induced AAN model mice (Fig. 1A). The chosen dosage of 84-B10 (10 mg·kg^{-1}) was based on previous studies [26, 27]. Serum biochemical results demonstrated that the AAI challenge led to a substantial increase in BUN and sCr levels, both of which were mitigated by 84-B10 (Figs. 1B−1C). Renal histological changes in AAI-exposed mice, including the loss of the proximal tubular brush border, tubular dilation, and cell cast formation, were observed. However, 84-B10 treatment significantly attenuated these histopathological alterations (Figs. 1D−1E). Furthermore, the study evaluated the mRNA and protein expression of NGAL, a sensitive biomarker of kidney injury, to confirm the AAN-alleviating effect of 84-B10. As shown in Fig. 1F, the transcription level of *Lcn2*, the gene encoding NGAL, significantly increased after AAI stimulation and was remarkably downregulated by 84-B10 therapy. The protein expression of NGAL exhibited similar results (Figs. 1G−1H).

Since AAN is also characterized by tubular cell apoptosis and immune cell infiltration [29], the investigation extended to evaluate the tissue expression of relevant apoptotic signaling molecules, notably BAX, as well as inflammatory factors, including CCL2, IL-1β, and IL-6. qRT-PCR and Western blotting analyses consistently revealed a marked increase in the expression of pro-apoptotic and pro-inflammatory molecules in response to AAI stimuli. Notably, the administration of 84-B10 efficiently mitigated the upregulation of these molecular markers (Figs. 1I−1K). These findings collectively underscore the therapeutic potential of 84-B10 in protecting against AAN in murine subjects.

Unbiased transcriptomic analysis of 84-B10 treated AAN model mice

To unravel the underlying mechanisms responsible for the protective effects of 84-B10 against AAN, we conducted an unbiased RNA-Seq analysis using kidney tissues obtained from AAN model mice treated with or without 84-B10. Our findings revealed substantial transcriptional alterations involving a total of 6957 genes, with 3640 genes upregulated and 3317 genes downregulated in the AAI group compared to the vehicle group. Furthermore, 608 genes exhibited transcriptional changes in the AAI + 84-B10 group compared to the AAI group, with 510 genes upregulated and 98 genes downregulated. We applied stringent criteria (fold change ≥ 1.5 or ≤ 0.67; *Q* value < 0.05) to define these changes (Fig. 2A). A Venn diagram analysis unveiled that 443 genes (con-

stituting about 73% of the total number of differentially expressed genes between the AAI + 84-B10 group and the AAI group) were concurrently down-regulated by AAI exposure and subsequently restored by 84-B10 treatment (Fig. 2B). Subsequent GO enrichment analysis conducted on these 443 genes highlighted the significant impact on the cellular components "mitochondrion" and "peroxisome" in the AAN kidney treated with 84-B10 (Fig. 2C). We further employed heatmaps to visually represent the clustered genes associated with the "mitochondrion" and "peroxisome" (Figs. S1 and S2, respectively). Collectively, our transcriptomic data underscore the therapeutic potential of 84-B10 in preserving the homeostasis of both mitochondria and peroxisomes.

84-B10 effectively restored AAI-induced mitochondrial dysfunction

To elucidate the effects of 84-B10 on mitochondrial structure and function, we employed TEM and various biochemical methods. Consistent with previous studies [30, 31], TEM analysis revealed significant mitochondrial damage in tubular cells following AAI administration, characterized by shortened length, disrupted cristae, incomplete membranes, and vacuole formation. Notably, treatment with 84-B10 significantly ameliorated these mitochondrial injuries (Figs. 3A−3B).

As cellular powerhouses, mitochondria generate ATP *via* the mitochondrial respiratory chain, which comprises five multi-subunit complexes (C I−C V). GSEA of transcriptomic data indicated that the mitochondrial respiratory chain was downregulated in the AAI group but reactivated upon 84-B10 treatment (Figs. 3C−3D). These transcriptomic findings were corroborated by the protein expression levels of key subunits of the mitochondrial respiratory chain, namely, C II-SDHB, C III-UQCRC2, and C V-ATP5A (Figs. 3E−3F). Mitochondrial fatty acid *β*-oxidation (mt-FAO) is crucial for ATP production in tubular epithelial cells. We assessed the expression of ACADM, the enzyme catalyzing the initial step of mt-FAO, and CPT2, responsible for transferring fatty acids into the mitochondrial matrix for *β*-oxidation. AAI exposure reduced the expression of ACADM and CPT2, but 84-B10 treatment significantly mitigated this reduction, indicating improved regulation of enzymes and proteins involved in mitochondrial fatty acid metabolism (Figs. 3G−3H). Additionally, the expression of SOD2, an enzyme responsible for detoxifying mitochondrial reactive oxygen species (mtROS), was reduced by AAI-induced injury but enhanced by 84-B10 treatment, suggesting an improved antioxidative capacity (Figs. 3G−3H).

We further investigated the impact of 84-B10 on mitochondrial protection in TKPT cells exposed to AAI. The CCK8 assay demonstrated a dose-dependent reduction in the viability of TKPT cells after 24-hour AAI exposure, with 5 μg·mL^{-1} of AAI chosen for subsequent experiments (Fig. 4A). We assessed the protective capacity of 84-B10 and found that concentrations of 20 and 30 μmol·L^{-1} partially restored cell viability following AAI exposure (Fig. 4B). For further experiments, we used 20 μmol·L^{-1} of 84-B10. To verify the mitochondrial protective effects of 84-B10 in TKPT cells, we examined the mtDNA copy number. AAI exposure reduced mtDNA copy numbers, but 84-B10 treatment

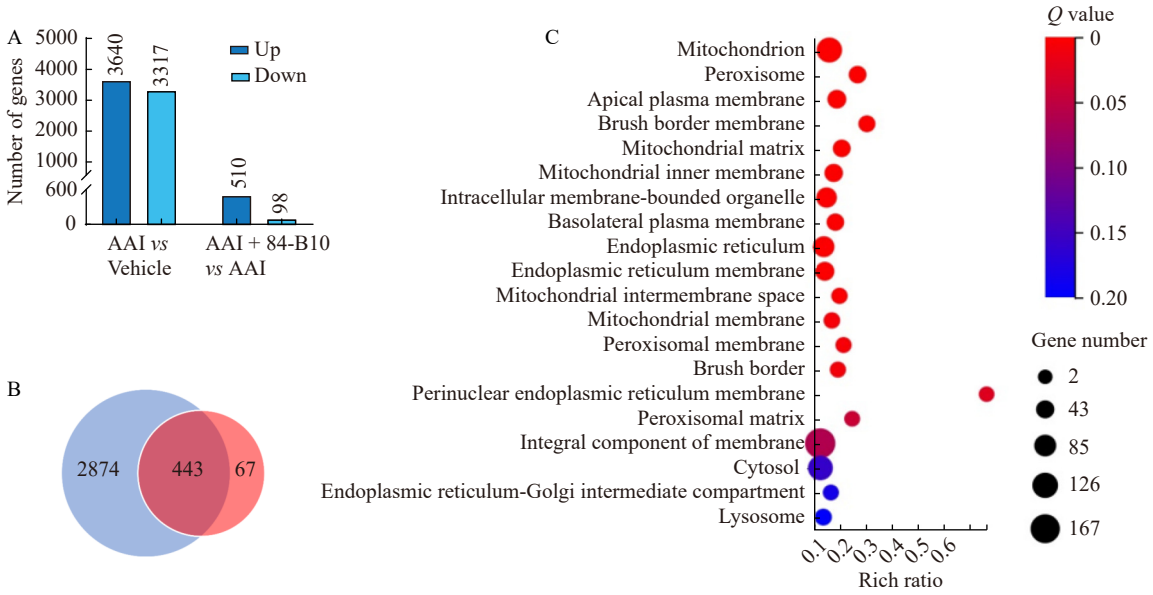

Fig. 2 RNA-seq analysis revealed that 84-B10 restored transcriptional signature associated with mitochondrion and peroxisome in AAN mice. (A) The number of genes showing transcriptional alterations when comparing the vehicle and AAI groups and when comparing the AAI + 84-B10 and AAI groups based on RNA-seq analysis (fold change ≥ 1.5 or ≤ 0.67; *Q* value < 0.05) (*n* = 3). (B) A Venn diagram displaying that 3317 genes were transcriptionally downregulated when comparing the AAI group to the vehicle group, while 510 genes were transcriptionally upregulated when comparing the AAI + 84-B10 group to the AAI group (fold change ≥ 1.5 or ≤ 0.67; *Q* value < 0.05) (*n* = 3). Among these genes, 443 were found to be in common. (C) GO cell component analysis revealed that the 443 overlapped genes were predominantly enriched in the categories of mitochondrion and peroxisome.

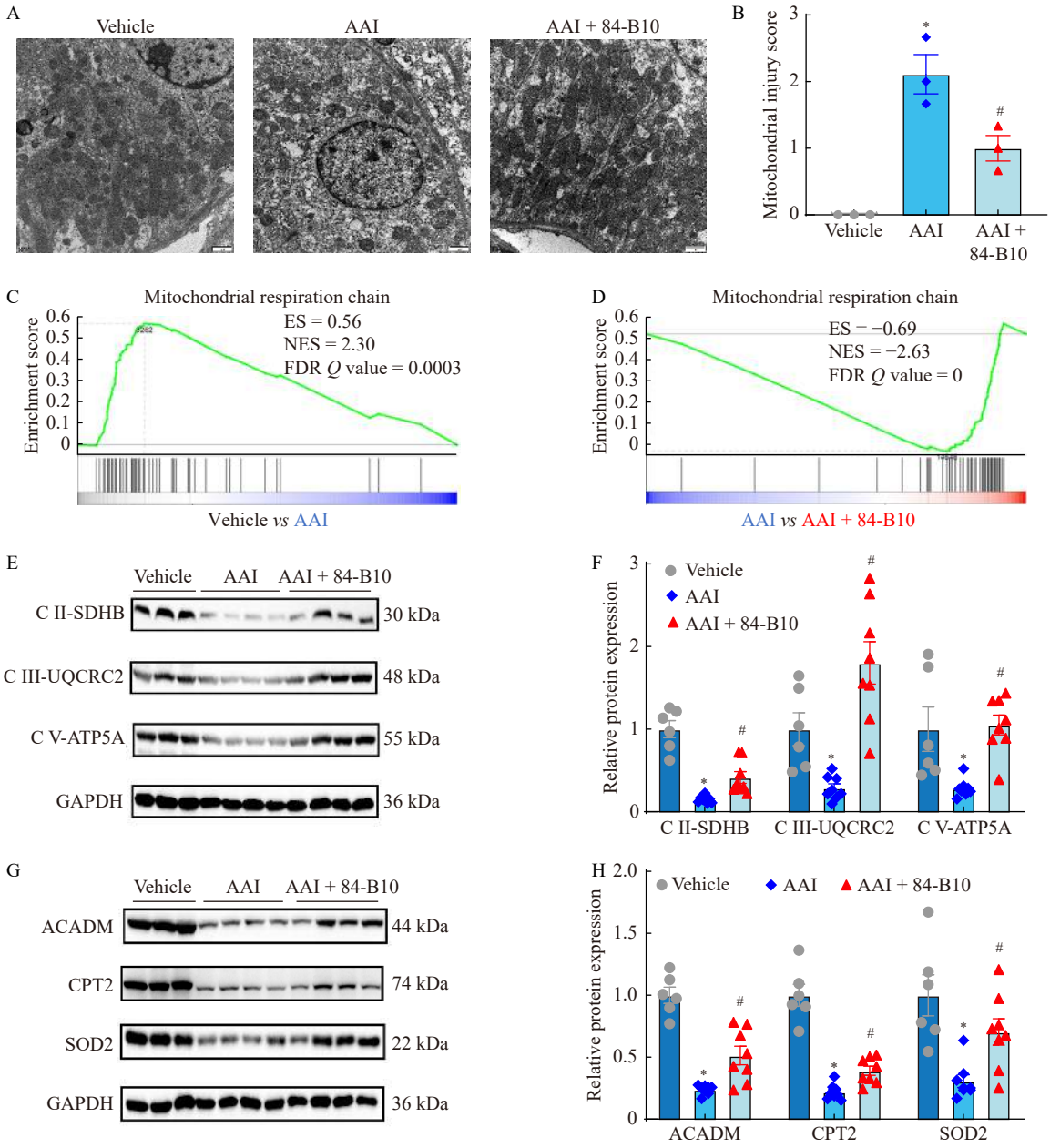

Fig. 3 84-B10 restored mitochondrial ultrastructure and function in AAN mice. (A) TEM images displaying the representative mitochondrial ultrastructure within tubular epithelial cells from each group. Scale bar = 500 nm. (B) Quantification of mitochondrial injury scores based on TEM analysis (n = 3). (C−D) GSEA illustrating the status of the mitochondrial respiration chain in comparisons between the vehicle and AAI groups and between the AAI and AAI + 84-B10 groups based on RNA-seq data (n = 3). ES, enrichment score; NES, normalized enrichment score; FDR, false discovery rate. (E−F) Representative immunoblots and semi-quantification of key mitochondrial respiration chain subunits, including C II-SDHB, C III-UQCRC2, and C V-ATP5A in kidney tissues (n = 6−8). (G) Representative immunoblots showing the expression of ACADM, CPT2 and SOD2 in kidney tissues. (H) Semi-quantification of the expression levels of ACADM, SOD2, and CPT2 based on Western blotting analysis in corresponding groups (n = 6−8). All data are presented as mean ± SEM. $^{*}P < 0.05$ *vs* the vehicle group; $^{\#}P < 0.05$ *vs* the AAI group.

significantly reversed this effect (Fig. 4C). Additionally, the transcription levels of twelve mtDNA-encoded genes, essential for the mitochondrial respiratory chain (C I subunits: *mt-Nd1*, *mt-Nd2*, *mt-Nd3*, *mt-Nd4*, *mt-Nd5*, and *mt-Nd6*; C III subunit: *Cytb*; C IV subunits: *mt-Co1*, *mt-Co2*, and *mt-Co3*; C V subunits: *mt-Atp6* and *mt-Atp8*), were largely restored by 84-B10 intervention following AAI exposure (Fig. 4D). In concordance with our *in vivo* findings, 84-B10 treatment improved mt-FAO in AAI-injured TKPT cells (Figs. 4E−4F). Mitochondrial dysfunction often results in increased mtROS, contributing to overall oxidative stress. We assessed mtROS and total ROS levels in TKPT cells and found significant increases in both due to AAI exposure. 84-B10 treatment efficiently reduced these ROS levels (Figs. 4G−4H). Notably, 84-

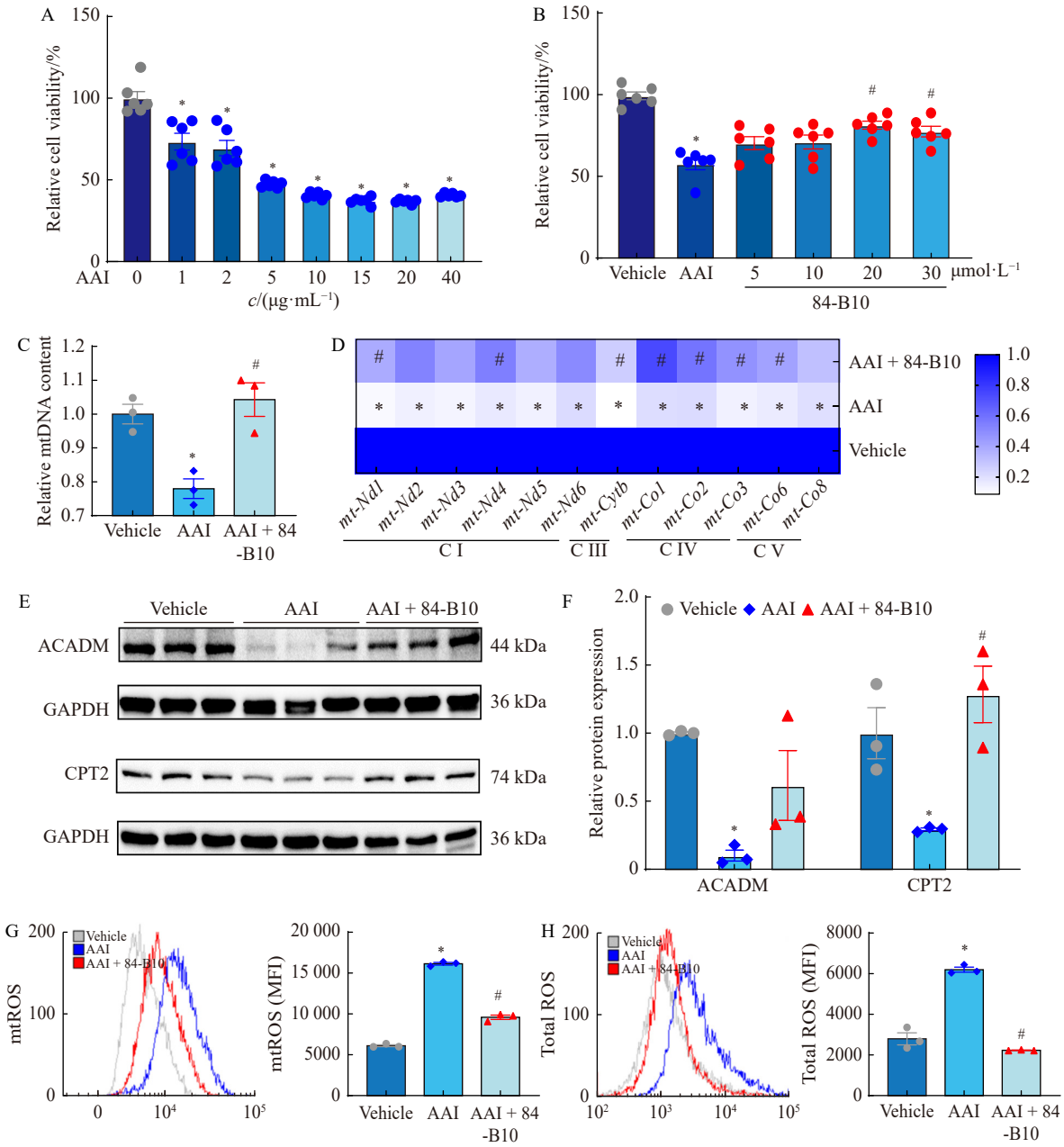

Fig. 4 84-B10 attenuated AAI-induced mitochondrial dysfunction in cultured kidney proximal tubular epithelial cells (A) TKPT cells were exposed to a range of AAI concentrations (1 to 40 μg·mL^{-1}) for 24 h, and cell viability was assessed using a CCK-8 assay (n = 6). (B) TKPT cells were pre-treated with 84-B10 (5–30 μmol·L^{-1}) for 2 h, followed by exposure to AAI (5 μg·mL^{-1}) for additional 12 h. Cell viability was measured using CCK-8 (n = 6). (C) TKPT cells were pre-treated with 84-B10 (20 μmol·L^{-1}) for 2 h, and then exposured to AAI (5 μg·mL^{-1}) for 12 h. The relative mtDNA copy number of TKPT cells was determined (n = 3). (D) TKPT cells were treated as in (C), and a heatmap illustrates the transcription levels of mitochondrial genes (*mt-Nd1*, *mt-Nd2*, *mt-Nd3*, *mt-ND4*, *mt-ND5*, *mt-ND6*, *Cytb*; *mt-Co1*, *mt-Co2*, *mt-Co3*, *mt-Atp6* and *mt-Atp8*) in TKPT cells based on qRT-PCR (n = 3). (E–F) TKPT cells were pre-treated with 84-B10 (20 μmol·L^{-1}) for 2 h before exposure to AAI (5 μg·mL^{-1}) for another 24 h. Western blots and semi-quantification of ACADM and CPT2 are presented (n = 3). (G) TKPT cells were treated as in (B). mtROS levels were estimated using a mitoSOX probe and analyzed *via* flow cytometry. Quantification of mtROS is displayed (n = 3); MFI, mean fluorescence intensity. (H) TKPT cells were treated as in (B). Total ROS levels were estimated by using a DCFH-DA probe and analyzed *via* flow cytometry. Quantification of total ROS is presented in parallel (n = 3). All data are presented as mean ± SEM. $^{*}P < 0.05$ *vs* the vehicle group; $^{\#}P < 0.05$ *vs* the AAI group.

B10 reduced total ROS to a greater extent than mtROS, suggesting that its protective effects might extend beyond mitochondrial homeostasis preservation (Figs. 4G–4H).

84-B10 alleviated AAI-induced peroxisomal dysfunction

GSEA, based on the RNA-seq data, also demonstrated a substantial disruption of peroxisomal function in AAI model

mice. Notably, this disruption was partially mitigated by treatment with 84-B10 (Figs. 5A−5B). To further validate the RNA-Seq findings, we evaluated the expression of transporters and enzymes that play pivotal roles in peroxisomal function, particularly peroxisomal fatty acid oxidation (per-FAO) and hydrogen peroxide (H_2O_2) clearance, both *in vivo* and *in vitro*. ACOX1 (encoded by *Acox1*) serves as the initial and rate-limiting enzyme of the per-FAO; ABCD3 (encoded by *Abcd3*) is a peroxisomal membrane protein acting as an ATP-dependent pump for fatty acid transport; and Catalase (encoded by *Cat*) is the most abundant peroxisomal enzyme responsible for H_2O_2 degradation. In response to AAI exposure, we observed a consistent reduction in the mRNA levels of *Acox1*, *Abcd3*, and *Cat* in mice, all of which were alleviated by 84-B10 treatment (Figs. 5C−5E). These trends were further confirmed by analyzing the protein expression of ACOX1 and Catalase (Figs. 5F−5G). Remarkably, we observed similar patterns in both mRNA and protein expression for these transporters and enzymes in AAI-injured TKPT cells upon 84-B10 treatment (Figs. 6A−6E). We also measured cellular H_2O_2 concentration and found that 84-B10 significantly reduced the heightened cellular H_2O_2 levels in AAI-challenged TKPT cells, suggesting an enhanced H_2O_2 clearance ability, particularly attributed to Catalase (Fig. 6F). Collectively, these findings underscore the detrimental impact of AAI on peroxisomes and highlight 84-B10's role in alleviating peroxisomal dysfunction under AAN conditions.

The tubular protective effect of 84-B10 under AAN condition is dependent on LONP1 activation

Previous studies have established 84-B10 as a potent activator of LONP1 [26]. In this study, we aimed to determine if the renoprotective effects of 84-B10 against AAN are dependent on LONP1 activation. Initially, we evaluated LONP1 expression in the AAN murine model. Our results demonstrated a significant downregulation of LONP1 following AAI exposure, which was substantially upregulated upon treatment with 84-B10 (Figs. 7A−7B). This outcome was consistently corroborated through immunofluorescence analysis of LONP1 in renal tissues (Figs. 7C−7D). Extending our

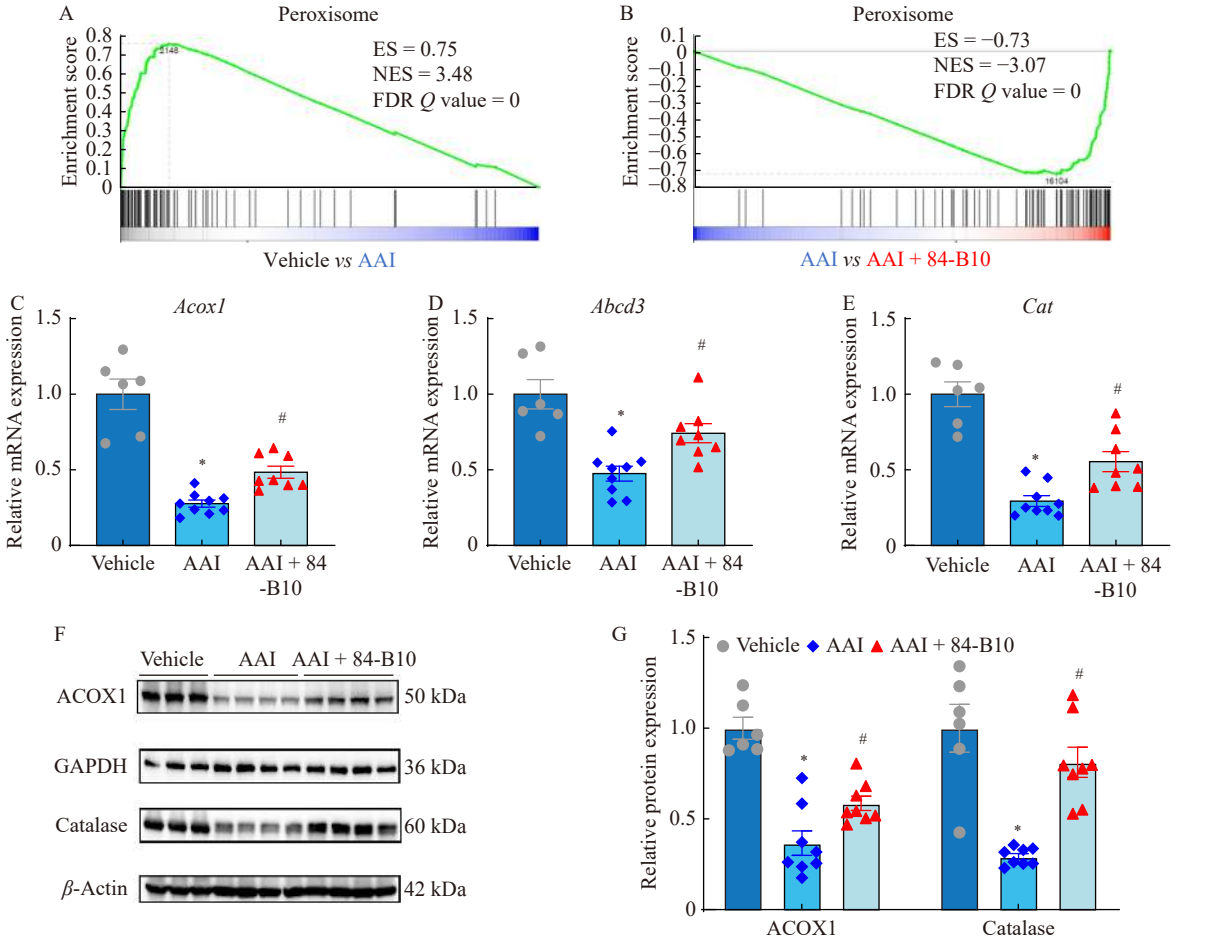

Fig. 5 Mitigation of AAN-associated peroxisomal dysfunction by 84-B10 in mice. (A−B) GSEA depicting the status of the peroxisome in comparisons between the vehicle and AAI groups and between the AAI and AAI + 84-B10 groups based on RNA-seq data (n = 3). ES, enrichment score; NES, normalized enrichment score; FDR, false discovery rate. (C−E) mRNA expression levels of *Acox1*, *Abcd3*, and *Cat* in kidney tissues (n = 6−9). (F−G) Representative immunoblots and semi-quantification of ACOX1 and Catalase in kidney tissues (n = 6−8). All data are presented as mean ± SEM. $^*P < 0.05$ *vs* the vehicle group; $^\#P < 0.05$ *vs* the AAI group.

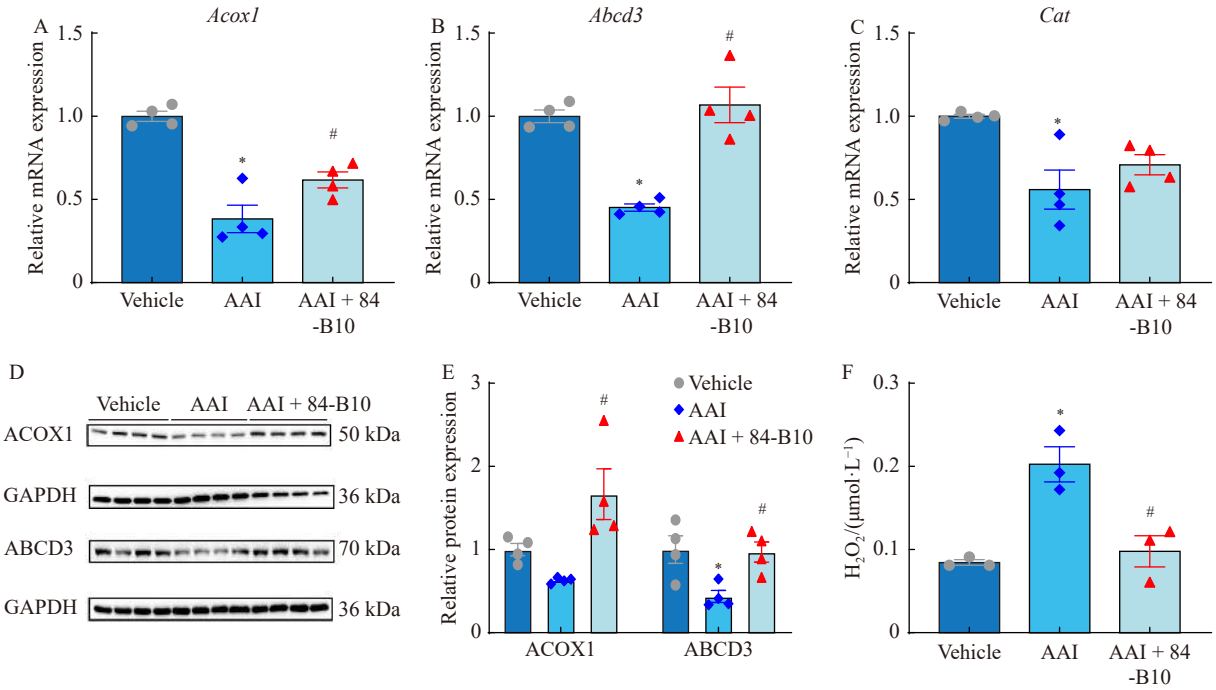

Fig. 6 84-B10 alleviated AAI-induced peroxisomal dysfunction in cultured kidney proximal tubular epithelial cells. (A−C) TKPT cells were pre-treated with 84-B10 (20 μmol·L^{-1}) for 2 h and exposed to AAI (5 μg·mL^{-1}) for another 12 h. The mRNA expression levels of *Acox1*, *Abcd3* and *Cat* were analyzed using qRT-PCR (n = 4). (D−E) TKPT cells were pre-treated with 84-B10 (20 μmol·L^{-1}) for 2 h and exposed to AAI (5 μg·mL^{-1}) for another 24 h. Protein expression of ACOX1 and ABCD3 in TKPT cells was estimated *via* Western blotting analysis. Semi-quantified of ACOX1 and ABCD3 is shown in (E) (n = 4). (F) TKPT cells were treated as in (A−C). The concentration of H_2O_2 in each group was estimated (n = 3). All data are presented as mean ± SEM. $^*P$ < 0.05 *vs* the vehicle group; $^\#P$ < 0.05 *vs* the AAI group.

investigation to AAI-challenged TKPT cells, we observed analogous results consistent with the *in vivo* data (Figs. 7E−7F). To explore the dependency of 84-B10's tubular protective effect on LONP1 activation, we utilized siRNAs to silence the *Lonp1* gene before administering 84-B10 treatment (Figs. 7G−7H). CCK8 assays revealed that the protective effect of 84-B10 on cell viability was significantly diminished following *Lonp1* knockdown (Fig. 7I). Additionally, the reduction in total ROS levels achieved by 84-B10 treatment was reversed after *Lonp1* knockdown (Fig. 7J). Collectively, these findings establish that the renal tubular protection afforded by 84-B10 in the context of AAN is contingent upon the activation of LONP1.

Discussion

Since the 1990s, researchers have uncovered the toxic nature of AAs, linking them to renal failure and urothelial carcinoma. Despite efforts such as the World Health Organization's classification of AAI as a Group 1 carcinogen [32] and the implementation of restrictions on AAs and AA-containing botanicals in various countries [33], the global population remains vulnerable due to the widespread use of medicinal plants containing AAs. Effective strategies to combat AA nephropathy (AAN) are still being sought.

LONP1 is an evolutionarily conserved serine peptidase that ensures mitochondrial proteostasis from yeast to humans [34]. Previously, our investigation revealed that decreased LONP1 expression plays an important role in mediating renal fibrosis [26]. By employing computer-aided virtual screening, we identified a novel LONP1 activator, 84-B10. Pharmacologically, 84-B10 mitigated mitochondrial dysfunction and attenuated renal fibrosis in various chronic kidney disease contexts [26]. We also found that 84-B10 can ameliorate cisplatin-induced acute kidney injury [27]. In the present study, we have extended our exploration to demonstrate the role of LONP1 and the protective efficacy of 84-B10 in AAN. Intriguingly, we observed a substantial reduction in LONP1 expression in the kidneys of mice and TKPT cells exposed to AAI, which was partially reversed by 84-B10 treatment. Along with the increased expression of LONP1, 84-B10 significantly attenuated renal dysfunction, mitigated renal histopathological alterations, and notably reduced the expression of the tubular injury marker NGAL in AAI-injured mice. Additionally, since tubular epithelial cell apoptosis and increased inflammation are pathological features of AAN, we evaluated tissue expression of the pro-apoptotic molecule BAX and pro-inflammatory factors, including CCL2, IL-1β, and IL-6. Results showed a reduction in apoptosis and inflammation levels after 84-B10 treatment. In an *in vitro* model utilizing TKPT, 84-B10 effectively preserved cell viability when exposed to AAI. However, when we knocked down

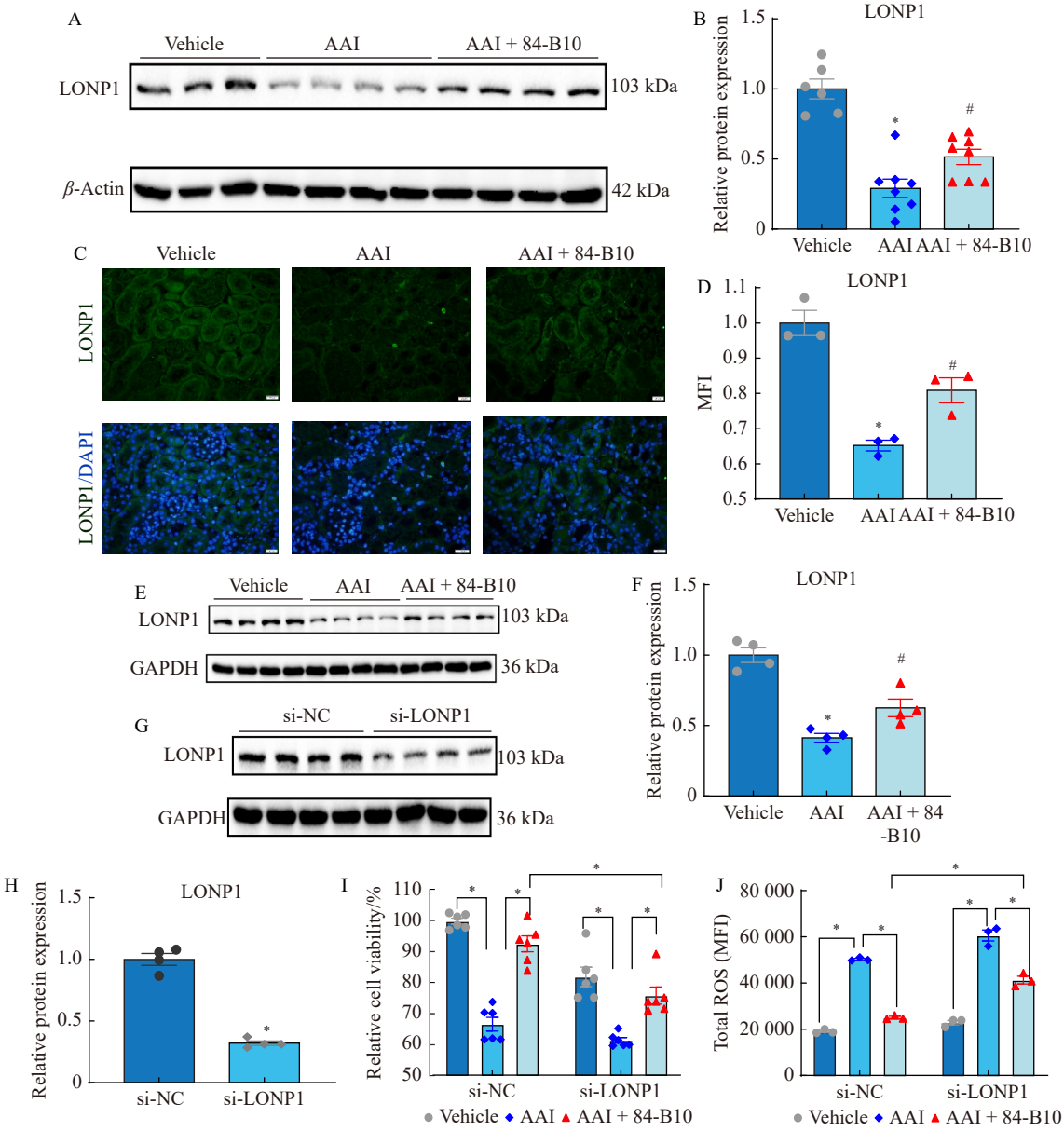

Fig. 7 The tubular protective effect of 84-B10 under the AAN condition was dependent on LONP1 activation. (A−B) Representative Western blots and semi-quantification of LONP1 in mouse kidney tissue (n = 6−8). (C−D) Immunofluorescence analysis of LONP1 in the cortex of mouse kidney. Scale bar = 20 μm. The mean fluorescence intensity (MFI) of LONP1 in each group is presented in (D) (n = 3). (E−F) TKPT cells were pre-treated with 84-B10 (20 μmol·L^{-1}) for 2 h and exposed to AAI (5 μg·mL^{-1}) for another 24 h. The protein expression of LONP1 in TKPT cells is shown (n = 4). (G-H) TKPT cells were transfected with scrambled siRNA (si-NC) or LONP1-targeted siRNAs (si-LONP1). Protein levels of LONP1 expression were analyzed *via* Western blotting analysis (n = 4). (I) TKPT cells were firstly transfected with si-NC or si-LONP1 and then pre-treated with 84-B10 (20 μmol·L^{-1}) for 2 h before exposure to AAI (5 μg·mL^{-1}) for another 24 h. Cell viability was assessed using a CCK-8 assay (n = 6). (J) TKPT cells were treated as in (I). Total ROS levels were measured using a DCFH-DA probe and analyzed by flow cytometry (n = 3). All data are presented as mean ± SEM. In Fig. B, D, F, H, $^{*}P < 0.05$ *vs* the vehicle group or si-NC group; $^{\#}P < 0.05$ *vs* the AAI group. In Figs. I−J, $^{*}P < 0.05$ between indicated groups.

Lonp1, the protective effect of 84-B10 on TKPT cell viability was significantly diminished. These findings suggest that 84-B10 protects tubular function under AAN conditions by activating LONP1, indicating that LONP1 may emerge as a promising target for the prevention and treatment of AAN.

Leveraging unbiased RNA-sequencing analysis, we identified that the genes downregulated by AAI exposure and ameliorated by 84-B10 treatment were primarily enriched in mitochondrial and peroxisomal functions. Given that 84-B10 is a potent LONP1 activator and mitochondrial protective agent and recognizing the close functional relationship between mitochondria and peroxisomes, we hypothesize that

84-B10 might play an advantageous role against AAN by maintaining the homeostasis of both mitochondria and peroxisomes.

Further biochemical analyses *in vivo* and *in vitro* demonstrated that 84-B10 preserves mitochondrial genomic integrity, protects the mitochondrial respiratory chain, alleviates dysregulation of key transporters and enzymes involved in mt-FAO, and reduces mtROS levels under AAI-induced stress. These findings underscore 84-B10's role as a guardian of mitochondrial function under various kidney-related stress conditions. Interestingly, 84-B10 exhibited a more potent ability to reduce total ROS levels compared to mtROS levels. Peroxisomes, which are ubiquitous intracellular organelles characterized by a single membrane, are especially abundant in renal tissue [35]. Beyond mitochondria, peroxisomes are critical sites for intracellular ROS generation and detoxification [19]. RNA-seq analysis and biochemical data suggest that 84-B10's protective role extends to maintaining peroxisomal homeostasis. Catalase, a key peroxisomal enzyme responsible for degrading H_2O_2, plays a vital role in maintaining cellular redox balance. Our investigation revealed that 84-B10 treatment restored Catalase expression and significantly reduced H_2O_2 levels in AAI-exposed TKPT cells. Thus, we propose that the restoration of peroxisomal antioxidative capacity by 84-B10, in conjunction with enhanced mitochondrial antioxidative systems, collectively contributes to the improvement of overall redox equilibrium.

In addition to their roles in ROS detoxification, peroxisomes and mitochondria exhibit shared functionalities in FAO. However, per-FAO and mt-FAO have notable distinctions regarding substrates, transport mechanisms, enzymatic reactions, and end products. Per-FAO primarily processes very long-chain and branched-chain fatty acids, relying on ATP-binding cassette (ABC) transporters, with the initial FAO reaction catalyzed by ACOXs. In contrast, mt-FAO primarily handles long-chain fatty acids, facilitated by the carnitine system involving CPT1 and CPT2. Per-FAO mainly participates in biosynthesis pathways, yielding H_2O_2 as the end product, whereas mt-FAO is associated with catabolism and energy production, coupling with the respiratory chain and the tricarboxylic acid cycle to generate adenosine triphosphate (ATP). Notably, these organelles collaborate in metabolizing very long-chain fatty acids, with peroxisomes generating a spectrum of chain-shortened acyl-coenzyme A molecules, including acetyl-CoA, propionyl-CoA, and various medium-chain acyl-CoAs, which are subsequently transferred to mitochondria for complete oxidation. In our experiments, we observed that AAI exposure profoundly decreased the levels of key enzymes and transporters involved in FAO in both mitochondria and peroxisomes. Treatment with 84-B10 significantly ameliorated these disruptions. These findings suggest that, in addition to its critical role in maintaining mitochondrial proteostasis, LONP1 may also play a significant role in peroxisomal homeostasis. However, it remains to be determined whether LONP1 serves as an adaptor facilitating physical interactions between mitochondria and peroxisomes or if it plays a role in signaling transduction pathways. Further investigations are necessary to elucidate the precise mechanisms by which LONP1 coordinates the activities of these two essential organelles.

In our previous study, we discovered that LONP1 targets 3-hydroxy-3-methylglutaryl-CoA synthase 2 (HMGCS2), a rate-limiting enzyme in ketogenesis, to protect mitochondrial function and mitigate chronic kidney disease [26]. To investigate the potential involvement of HMGCS2 in AAN, we evaluated its expression in mouse kidneys. Our results showed that HMGCS2 expression was upregulated in AAN kidneys (Figs. S3A−S3B). However, 84-B10 treatment did not affect HMGCS2 expression in AAI-injured kidneys (Figs. S3A−S3B), suggesting that HMGCS2 is not responsible for the therapeutic effects of 84-B10 in AAN. We also performed a detailed analysis of genes with opposing expression patterns. Venn diagram analysis revealed 86 genes that were upregulated by AAI exposure and subsequently downregulated by 84-B10 treatment (Fig. S4A). KEGG enrichment analysis of these genes identified significant pathways, including "cell adhesion molecules" and "cytokine-cytokine receptor interaction" (Fig. S4B). Heatmaps indicated that six genes clustered in the "cell adhesion molecules" pathway and seven genes clustered in the "cytokine-cytokine receptor interaction" pathway (Figs. S4C−S4D). These genes are primarily involved in inflammatory processes by facilitating the adhesion, attraction, and activation of immune cells such as macrophages, monocytes, and leukocytes [36-39]. The downregulation of these genes following 84-B10 treatment may indicate a secondary response, though their direct contributions to AAN require further investigation.

Our study highlights the interconnected regulation of mitochondria and peroxisomes, as dysfunction in one organelle can lead to dysfunction in the other [21]. It is essential to address both organelles when considering cellular stress conditions. The 3-phenylglutaric acid derivative 84-B10 shows promise as a therapeutic agent against AAN due to its ability to activate LONP1 and ameliorate dysfunctions in both mitochondria and peroxisomes in rodent and cell-based models. However, further exploration of its clinical applications is still in need.

Conclusion

In summary, our study provides compelling evidence that AAN is characterized by significant disruptions in both mitochondrial and peroxisomal functions. Notably, the LONP1 activator 84-B10 has demonstrated remarkable efficacy in alleviating AAN, primarily through the restoration of mitochondrial and peroxisomal homeostasis (Fig. 8). These findings underscore the therapeutic potential of 84-B10 in addressing the multifaceted cellular dysfunctions associated with AAN.

Supporting Information

The raw data files and processed data from the transcrip-

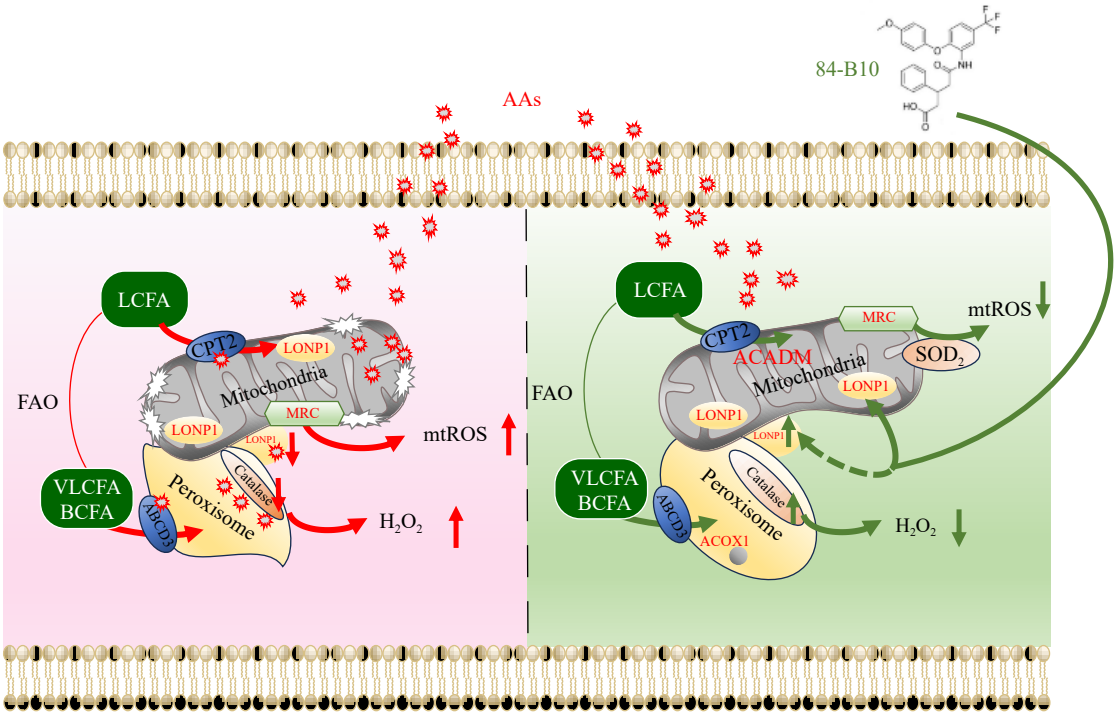

Fig. 8 Proposed mechanism of 84-B10 in protecting against AAN. AAs preferentially affect tubular epithelial cells, leading to mitochondrial and peroxisomal damage. Treatment with the LONP1 activator 84-B10 safeguards mitochondrial ultrastructure, restores mitochondrial respiration, mitochondrial fatty acid *β*-oxidation, and mitigates mitochondrial ROS in AAs-injured proximal tubular epithelial cells. Simultaneously, 84-B10 protects peroxisomal fatty acid *β*-oxidation and enhances peroxisomal catalase activity for the clearance of H_2O_2. This multifaceted protective mechanism contributes to the mitigation of AAN. LCFA, long-chain fatty acids; VLCFA, very long-chain fatty acids; BCFA, branched-chain fatty acids; MRC, mitochondrial respiration chain.

tional analysis of kidney tissues have been deposited in the NCBI Gene Expression Omnibus (GEO) database and can be accessed at GSE245755. To access the data, please use the secure token number: wjuveiuidtifhul. All other supporting data can be requested by sending E-mail to the corresponding authors.

Declaration of Generative AI and AI-assisted technologies in the writing process

During the preparation of this work the authors used Chatgpt in order to improve readability and language. After using this tool, the authors reviewed and edited the content as needed and take full responsibility for the content of the publication.

References

[1] Das S, Thakur S, Korenjak M, *et al*. Aristolochic acid-associated cancers: a public health risk in need of global action [J]. *Nat Rev Cancer*, 2022, **22**(10): 576-591.

[2] Zhang Q, Luo P, Chen J, *et al*. Dissection of targeting molecular mechanisms of aristolochic acid-induced nephrotoxicity *via* a combined deconvolution strategy of chemoproteomics and metabolomics [J]. *Int J Biol Sci*, 2022, **18**(5): 2003-2017.

[3] Li P, Pit WN, Lean YL, *et al*. Herbal products containing aristolochic acids: a call to revisit the context of safety [J]. *J Herb Med*, 2021, **28**: 100447.

[4] De Araújo F, Nogueira C, Trichez V, *et al*. Anti-hyperglycemic potential and chemical constituents of *Aristolochia triangularis* Cham. leaves−a medicinal species native to Brazilian forests [J]. *J Ethnopharma Col*, 2023, **303**: 115991.

[5] Yang B, Xie Y, Guo M, *et al*. Nephrotoxicity and Chinese herbal medicine [J]. *Clin J Am Soc Nephrol*, 2018, **13**(10): 1605-1611.

[6] Gökmen M, Cosyns J, Arlt V, *et al*. The epidemiology, diagnosis, and management of aristolochic acid nephropathy: a narrative review [J]. *Ann Intern Med*, 2013, **158**(6): 469-477.

[7] Anandagoda N, Lord G. Preventing aristolochic acid nephropathy [J]. *Clin J Am Soc Nephrol*, 2015, **10**(2): 167-168.

[8] Ren J, Rudemiller NP, Wen Y, *et al*. The transcription factor Twist1 in the distal nephron but not in macrophages propagates aristolochic acid nephropathy [J]. *Kidney Int*, 2020, **97**(1): 119-129.

[9] Wang X, Xue N, Zhao S, *et al*. Upregulation of miR-382 contributes to renal fibrosis secondary to aristolochic acid-induced kidney injury *via* PTEN signaling pathway [J]. *Cell Death Dis*, 2020, **11**(8): 620.

[10] Baudoux TE, Pozdzik AA, Arlt VM, *et al*. Probenecid prevents acute tubular necrosis in a mouse model of aristolochic acid nephropathy [J]. *Kidney Int*, 2012, **82**(10): 1105-1113.

[11] Wang Y, Liu Z, Ma J, *et al*. Lycopene attenuates the inflammation and apoptosis in aristolochic acid nephropathy by targeting the Nrf2 antioxidant system [J]. *Redox Biol*, 2022, **57**: 102494.

[12] Jin C, Miao X, Zhong Y, *et al*. The renoprotective effect of diosgenin on aristolochic acid I-induced renal injury in rats: impact on apoptosis, mitochondrial dynamics and autophagy [J]. *Food Funct*, 2020, **11**(9): 7456-7467.

[13] Jo DS, Park NY, Cho DH. Peroxisome quality control and dys-

regulated lipid metabolism in neurodegenerative diseases [J]. *Exp Mol Med*, 2020, **52**(9): 1486-1495.
[14] Di Cara F, Savary S, Kovacs WJ, *et al*. The peroxisome: an up-and-coming organelle in immunometabolism [J]. *Trends in Cell Biology*, 2023, **33**(1): 70-86.
[15] Wanders RJ, Waterham HR. Biochemistry of mammalian peroxisomes revisited [J]. *Annu Rev Biochem*, 2006, **75**: 295-332.
[16] Braverman NE, D'Agostino MD, Maclean GE. Peroxisome biogenesis disorders: biological, clinical and pathophysiological perspectives [J]. *Dev Disabil Res Rev*, 2013, **17**(3): 187-196.
[17] Lodhi IJ, Semenkovich CF. Peroxisomes: a nexus for lipid metabolism and cellular signaling [J]. *Cell Metab*, 2014, **19**(3): 380-392.
[18] Schrader M, Kamoshita M, Islinger M. Organelle interplay-peroxisome interactions in health and disease [J]. *J Inherit Metab Dis*, 2020, **43**(1): 71-89.
[19] Vasko R. Peroxisomes and kidney injury [J]. *Antioxid Redox Signal*, 2016, **25**(4): 217-231.
[20] Vasko R, Ratliff BB, Bohr S, *et al*. Endothelial peroxisomal dysfunction and impaired pexophagy promotes oxidative damage in lipopolysaccharide-induced acute kidney injury [J]. *Antioxid Redox Signal*, 2013, **19**(3): 211-230.
[21] Wanders R, Baes M, Ribeiro D, *et al*. The physiological functions of human peroxisomes [J]. *Physiol Rev*, 2023, **103**(1): 957-1024.
[22] Wozny M, Di Luca A, Morado D, *et al*. *In situ* architecture of the ER-mitochondria encounter structure [J]. *Nature*, 2023, **618**(7963): 188-192.
[23] Shai N, Yifrach E, van Roermund C, *et al*. Systematic mapping of contact sites reveals tethers and a function for the peroxisome-mitochondria contact [J]. *Nat Commun*, 2018, **9**(1): 1761.
[24] Mattiazzi Usaj M, Brloznik M, Kaferle P, *et al*. Genome-wide localization study of yeast Pex11 identifies peroxisome-mitochondria interactions through the ERMES complex [J]. *J Mol Biol*, 2015, **427**(11): 2072-2087.
[25] Li Y, Huang D, Jia L, *et al*. Lonp1 links mitochondria-ER interaction to regulate heart function [J]. *Research (Wash DC)*, 2023, **6**: 715.
[26] Bai M, Wu M, Jiang M, *et al*. LONP1 targets HMGCS2 to protect mitochondrial function and attenuate chronic kidney disease [J]. *EMBO Mol Med*, 2023, **15**(2): e16581.
[27] Fan J, Xu X, Li Y, *et al*. A novel 3-phenylglutaric acid derivative (84-B10) alleviates cisplatin-induced acute kidney injury by inhibiting mitochondrial oxidative stress-mediated ferroptosis [J]. *Free Radic Biol Med*, 2023, **194**: 84-98.
[28] Su M, Liu X, Zhao Y, *et al*. *In silico* and *in vivo* pharmacokinetic evaluation of 84-B10, a novel drug candidate against acute kidney injury and chronic kidney disease [J]. *Molecules*, 2023, **29**(1): 159.
[29] Chen J, Luo P, Wang C, *et al*. Integrated single-cell transcriptomics and proteomics reveal cellular-specific responses and microenvironment remodeling in aristolochic acid nephropathy [J]. *JCI Insight*, 2022, **7**(16): e157360.
[30] Pozdzik AA, Salmon IJ, Debelle FD, *et al*. Aristolochic acid induces proximal tubule apoptosis and epithelial to mesenchymal transformation [J]. *Kidney Int*, 2008, **73**(5): 595-607.
[31] Kayhan M, Vouillamoz J, Rodriguez DG, *et al*. Intrinsic TGF-β signaling attenuates proximal tubule mitochondrial injury and inflammation in chronic kidney disease [J]. *Nat Commun*, 2023, **14**(1): 3236.
[32] IARC Working Group on the Evaluation of Carcinogenic Risks to Humans. Some traditional herbal medicines, some mycotoxins, naphthalene and styrene [J]. *ARC Monogr Eval Carcinog Risks Hum*, 2002, **82**: 1-556.
[33] Xian Z, Tian J, Zhang Y, *et al*. Study on the potential nephrotoxicity and mutagenicity of aristolochic acid IVa and its mechanism [J]. *Biomed Pharmacother*, 2021, **142**: 112081.
[34] Deshwal S, Fiedler KU, Langer T. Mitochondrial proteases: multifaceted regulators of mitochondrial plasticity [J]. *Annu Rev Biochem*, 2020, **89**: 501-528.
[35] Gabaldon T. Peroxisome diversity and evolution [J]. *Philos Trans R Soc Lond B Biol Sci*, 2010, **365**(1541): 765-773.
[36] Xu L, Sharkey D, Cantley LG. Tubular GM-CSF promotes late MCP-1/CCR2-mediated fibrosis and inflammation after ischemia/reperfusion injury [J]. *J Am Soc Nephrol*, 2019, **30**(10): 1825-1840.
[37] Lu C, Lei W, Sun M, *et al*. Identification of CCR2 as a hub in septic myocardial injury and cardioprotection of silibinin [J]. *Free Radic Biol Med*, 2023, **197**: 46-57.
[38] Helmke A, Nordlohne J, Balzer MS, *et al*. CX3CL1-CX3CR1 interaction mediates macrophage-mesothelial cross talk and promotes peritoneal fibrosis [J]. *Kidney Int*, 2019, **95**(6): 1405-1417.
[39] Gu X, Weng R, Hou J, *et al*. Endothelial miR-199a-3p regulating cell adhesion molecules by targeting mTOR signaling during inflammation [J]. *Eur J Pharmacol*, 2022, **925**: 174984.

Cite this article as: XU Xinyue, ZHU Wenping, MIAO Mengqiu, *et al*. Activation of LONP1 by 84-B10 alleviates aristolochic acid nephropathy *via* re-establishing mitochondrial and peroxisomal homeostasis [J]. *Chin J Nat Med*, 2024, **22**(9): 808-821.